Optimization of Microstructure and Mechanical Properties of Co Cr Mo Alloys by High-Pressure Torsion and Subsequent Short Annealing

doi: 10.2320/matertrans.M2016112

Materials Transactions, Vol. 57, No. 11 (2016) pp. 1887 to 1896

Optimization of Microstructure and Mechanical Properties of Co–Cr–Mo Alloys by High-Pressure Torsion and Subsequent Short Annealing

Murat Isik[1,*1], Mitsuo Niinomi[2,*2], Huihong Liu[3], Ken Cho[4], Masaaki Nakai[2], Zenji Horita[5,6], Takayuki Narushima[7] and Kyosuke Ueda[7]

[1]*Department of Materials Science, Tohoku University, Sendai 980–8579, Japan*
[2]*Institute for Materials Research, Tohoku University, Sendai 980–8577, Japan*
[3]*Joining and Welding Research Institute, Osaka University, Ibaraki 567–0047, Japan*
[4]*Graduate School of Engineering, Osaka University, Suita 565–0871, Japan*
[5]*Department of Materials Science and Engineering, Faculty of Engineering, Kyushu University, Fukuoka 819–0395, Japan*
[6]*WPI, International Institute for Carbon-Neutral Energy Research (WPI-I2CNER), Kyushu University, Fukuoka 819–0395, Japan*
[7]*Department of Materials Processing, Tohoku University, Sendai 980–8579, Japan*

The main target of this study is to optimize the microstructure and to achieve an optimization for the mechanical properties in a biomedical Co-Cr-Mo (CCM) alloy with the nominal composition of Co–28Cr–6Mo (mass%) subjected to high-pressure torsion (HPT) and subsequent short annealing. The $\gamma \rightarrow \varepsilon$ phase transformation and grain refinement occur in the CCM alloy subjected to HPT processing at an equivalent strain (ε_{eq}) of 2.25 (CCM_{HPT}). The HPT processing causes a decrease in the elongation due to the formation of an excessive amount of ε phase. For removal of the excessive amount of ε phases, the CCM_{HPT} was subjected to a short annealing (CCM_{HPTA}). The effect of the short annealing temperature (1073 K, 1273 K, and 1473 K; annealing time was fixed at 0.3 ks) on CCM_{HPT} was investigated. In addition, the effect of the length of duration for the short annealing (0.06 ks, 0.3 ks, and 0.6 ks;) for a fixed annealing temperature of 1273 K on CCM_{HPT} was studied. $CCM_{HPTA(1273\ K)}$ annealed for 0.3 ks shows a good optimization of mechanical properties that include high strength and large elongation owing to its ultrafine-grained microstructure, and removal of excessive ε phases. [doi:10.2320/matertrans.M2016112]

(Received March 28, 2016; Accepted August 24, 2016; Published September 30, 2016)

Keywords: *cobalt-chromium-molybdenum alloys, biomaterials, high-pressure torsion, grain refinement, short annealing*

1. Introduction

CCM alloys have been widely used as implant materials in biomedical applications such as hip and knee joints because of their excellent mechanical properties and good biocompatibility.[1–3] The mechanical properties of CCM alloys need to be further improved to reduce the probability of failure in biomedical applications.[4] Grain refinement is effective to improve the mechanical properties of CCM alloys. In fact, CCM alloys with small grain size have been practically used.[5] It has been reported that hot forging[6] can refine the CCM grains from an initial size of 40 μm to 0.6 μm.[6] However, grain refinement to a nano-scale is difficult to be achieved by the conventional processing methods.

The processing of metals with severe plastic deformation offers the potential for achieving extraordinary grain refinement in metals.[7] Several severe plastic deformation methods have been utilized so far, and among them most interest has been placed on equal-channel angular pressing (ECAP)[8,9] and high-pressure torsion (HPT).[10] In general, processing by ECAP, where a rod is pressed through a die constrained within a channel, causes grain refinement on the micrometer scale,[8] while HPT processing, where a disk is subjected to a high applied pressure and torsional straining, causes grains to be refined on the nanometer level.[7,10] The large numbers of dislocations introduced by HPT processing rearrange and aggregate to form dislocation cells. Subsequently, the dislocation rearrangement increases the misorientation between the cells thereby causing the formation of low-angle and then high-angle grain boundaries.[9–11] In addition, HPT processing, which can induce a very high strain,[12] may cause phase transformations in some metallic materials. It has been known that inducing a high strain can cause $\gamma \rightarrow \varepsilon$ transformation in Co-Cr-Mo (CCM) alloys.[13]

It has been reported that HPT processing can significantly improve the strength of the CCM alloy via the $\gamma \rightarrow \varepsilon$ strain-induced martensitic transformation and grain refinement. However, HPT processed CCM alloys generally exhibit poor elongation[14] even some previous studies report that ductility of ε phase is not necessarily inferior to that of γ phase[15,16] but transformed ε phases can act as obstacles for pinning the dislocation gliding. Furthermore, an ε phase with an hcp structure has limited slip systems, whereby it generally shows low ductility compared to that of γ phase. Therefore poor elongation of HPT-processed CCM alloy is considered to be attributed to the excessive ε phase. Thus, it is necessary to improve the elongation of the HPT-processed CCM alloy while keeping its strength still high.

A short annealing is expected to induce a recovery in the elongation and maintain a high tensile strength in the HPT-processed CCM alloy by optimizing the volume fraction and distribution of the ε phase while keeping the ultrafine-grained microstructure in the alloy.

In this study, the aim was to obtain optimized mechanical properties in the CCM alloy as a combination of high strength and large elongation by means of conducting a short annealing after HPT processing. The short annealing conditions including temperature and time were optimized. The effects of short annealing temperature and time on the microstructure and mechanical properties of the HPT processed CCM alloy were comprehensively investigated.

[*1]Graduate Student, Tohoku University
[*2]Corresponding author, E-mail: niinomi@imr.tohoku.ac.jp

2. Experimental Procedures

2.1 Material preparation

A cylindrical rod of a hot forged CCM alloy with a nominal composition of Co–28Cr–6Mo (mass%) alloy with a diameter of 25 mm and a length of 50 mm was used in this study. The chemical composition of the CCM alloy is listed in Table 1. The rod was subjected to solution treatment at 1473 K for 3.6 ks in vacuum (hereafter designated as CCM_{ST}). The CCM_{ST} rod was machined to disk-shaped specimens with diameters of 10 mm and thicknesses of 1 mm for HPT processing. The CCM_{ST} disk was subjected to HPT processing under quasi-constrained conditions, in which the lower anvil was rotated 0.25 times with a rotation speed of 1 rpm (0.1220 rad s^{-1}) under a pressure of 6 GPa in air at room temperature (hereafter designated as CCM_{HPT}). Then, the CCM_{HPT} was subjected to a short annealing (hereafter designated as CCM_{HPTA}). The short annealings (duration was fixed at 0.3 ks) were conducted at 1073 K ($CCM_{HPTA(1073\ K)}$), 1273 K ($CCM_{HPTA(1273\ K)}$), and 1473 K ($CCM_{HPTA(1473\ K)}$) in order to investigate the effect of short annealing temperature on CCM_{HPT}. In addition, the short annealings (temperature was fixed at 1273 K) were conducted for 0.06 ks ($CCM_{HPTA(0.06\ ks)}$), 0.3 ks ($CCM_{HPTA(0.3\ ks)}$), and 0.6 ks ($CCM_{HPTA(0.6\ ks)}$) for studying the effect of short annealing duration on CCM_{HPT}. Hereafter, the CCM alloy subjected to HPT and subsequent annealing at the temperature T for the duration of t, is designated by $CCM_{HPTA(T/t)}$ as $CCM_{HPTA(1273\ K,0.3\ ks)}$ for the case of T = 1273 K and t = 0.3 ks. The equivalent strain ε_{eq} at a distance r from the disk center was estimated by the following equation:[10)]

$$\varepsilon_{eq} = 2\pi rN/t\sqrt{3} \quad (1)$$

where N is the rotation number and t is the specimen thickness. ε_{eq} was calculated according to eq. (1), as a function of distance from the disk center for N = 0.25. As a result, the value of ε_{eq} is 2.25 for N = 0.25 at the half radius, r_h (r = 2.5 mm). Additionally, CCM_{ST} disks were also subjected to cold rolling with a thickness reduction of 50% (ε_{eq} = 0.8)[17)] (hereafter designated as CCM_{CR}).

Table 1 Chemical composition of hot forged CCM alloy (mass%).

Element	Cr	Mo	Ni	Mn	Si	C	N	Fe	Co
	27.7	5.87	<0.01	0.58	0.50	0.045	0.14	<0.1	Bal.

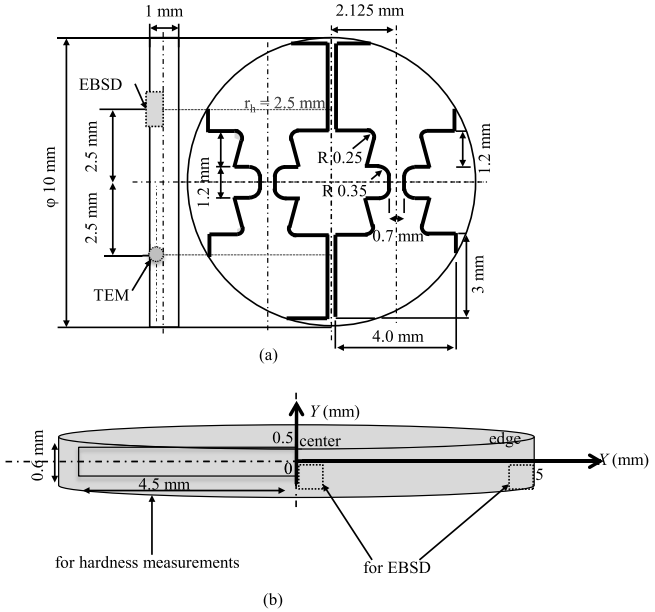

Fig. 1 (a) Positions for EBSD and TEM analyses and geometry of tensile test specimen and (b) hardness measurement positions for cross section of disk sample and EBSD analyses positions corresponding to hardness measurements.

2.2 Microstructural characterization

The microstructures of specimens were characterized by electron backscatter diffraction analysis (EBSD) and transmission electron microscopy (TEM) using an accelerating voltage of 200 kV. The EBSD and TEM analyses were carried out at r_h, which is 2.5 mm away from the disk center, as shown schematically in Fig. 1(a). Additionally, EBSD analyses were carried out at the center and edge of the cross section of the specimen, as shown in Fig. 1 (b). The specimens for EBSD analysis were wet-polished using water-proof emery papers up to #2400 and were then buff-polished to obtain a mirror surface by a colloidal SiO_2 suspension. For TEM sample preparation, the sample disk was fixed between two silicon substrates using an epoxy resin and then a thin plate was cut parallel to the cross section near the center of the disk sample. The plate was wet polished using water-proof emery papers up to #2400. Then, a copper ring with a diameter of 3 mm was fixed on the polished plate at the r_h position using an epoxy resin. The thin plate was further thinned to less than 20 μm using a dimple grinder and an ion-milling apparatus. Additional information about the TEM sample preparation was described and illustrated in details in a previous study.[11)]

2.3 Mechanical tests

An Instron-type testing machine was used for evaluating the tensile properties of the CCM alloys. The tensile tests were conducted at room temperature with a cross-head speed of 8.33×10^{-6} m·s^{-1}, which is equivalent to an initial strain rate of 6.94×10^{-3} s^{-1}. The tensile specimens were obtained from disk-shaped samples and the schematic drawing, is shown in Fig. 1 (a).[14)] The tensile specimens were cut using a FANUC electric-discharge machine. The tensile specimens were wet-polished using water-proof emery papers up to #1500 and thinned to a cross-sectional thickness of 0.5–0.6 mm (i.e., material up to a depth of ~0.2–0.25 mm was removed from both surfaces of the specimen).

Hardness measurements were carried out using a Vickers microhardness tester with a load of 4.9 N for a dwell time of 15 s on the surface of the specimens. The measurements on the cross section of the disk-shaped specimen were performed at the interval of 0.5 mm and 0.15 mm between the measurement positions in the radial direction and cross section depth direction.

3. Results

3.1 Effects of short annealing temperature

Figure 2 shows the EBSD phase map, inverse pole figure (IPF) map, kernel average misorientation (KAM) maps, the

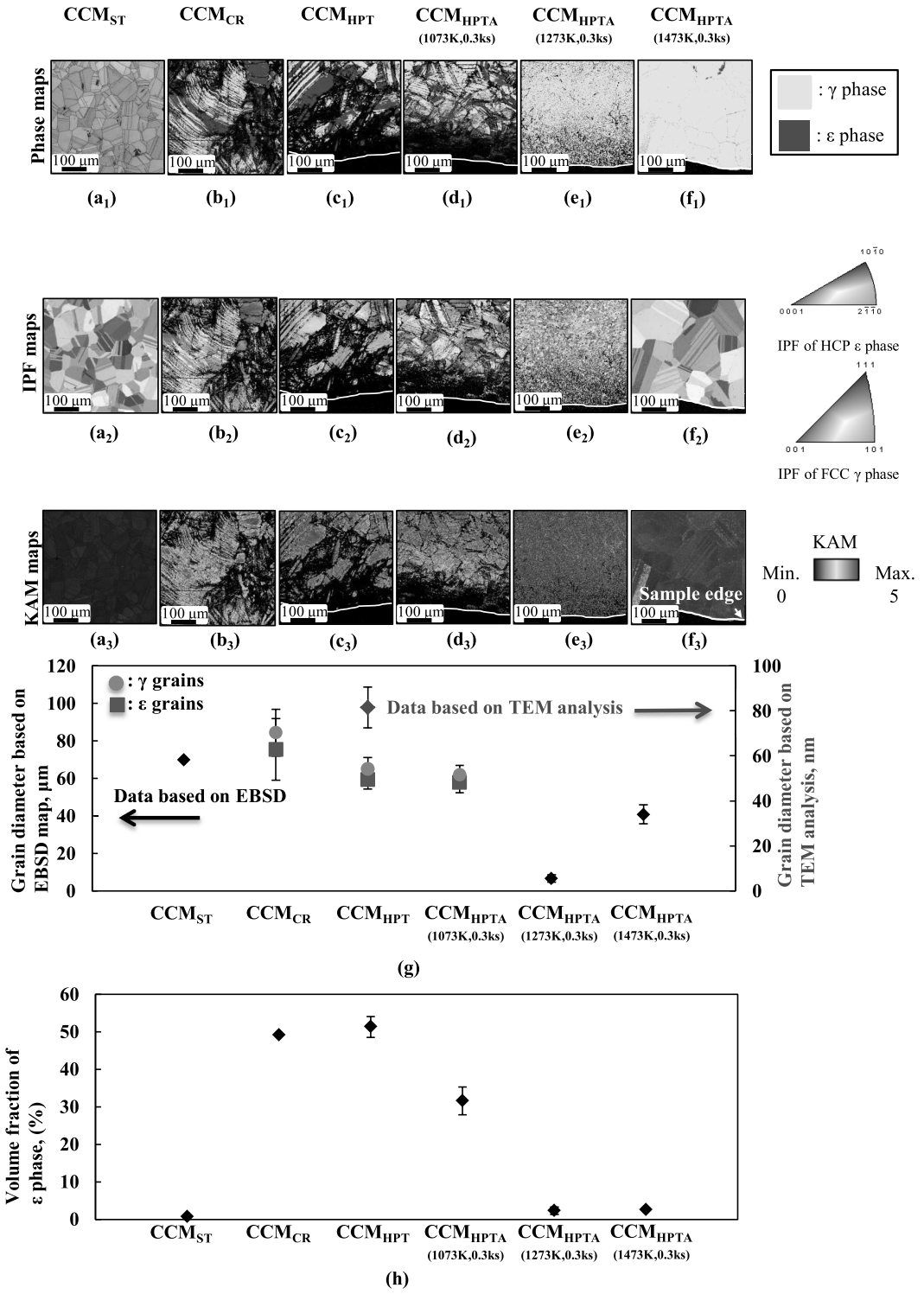

Fig. 2 EBSD ((a$_1$)–(f$_1$)) phase, ((a$_2$)–(f$_2$)) IPF and ((a$_3$)–(f$_3$)) KAM maps and (g) average grain diameter, and (h) volume fraction of ε phases of CCM_{ST}, CCM_{CR}, CCM_{HPT}, $CCM_{HPTA(1073\ K,0.3\ ks)}$, $CCM_{HPTA(1273\ K,0.3\ ks)}$, and $CCM_{HPTA(1473\ K,0.3\ ks)}$ based on EBSD analysis.

average grain diameter, and volume fractions of ε phases of CCM_{ST}, CCM_{CR}, CCM_{HPT}, and $CCM_{HPTA(1073\ K)}$, $CCM_{HPTA(1273\ K)}$, and $CCM_{HPTA(1473\ K)}$ for 0.3 ks. The EBSD phase maps show that CCM_{ST} consists almost entirely of a face centered cubic (fcc) γ phase, whereas CCM_{HPT}, $CCM_{HPTA(1073\ K)}$, $CCM_{HPTA(1273\ K)}$, and $CCM_{HPTA(1473\ K)}$ have dual-phase microstructure, composed of the γ and hexagonal close packed (hcp) ε phase.

It has been reported that volume fraction of ε phase is around 87% based on X-ray diffraction (XRD) analysis in CCM_{HPT}[18]. Volume fraction of ε phase in $CCM_{HPTA(1073\ K,0.3\ ks)}$ (~31%) is higher than those in $CCM_{HPTA(1273\ K,0.3\ ks)}$ and $CCM_{HPTA(1473\ K,0.3\ ks)}$ (~2%), and lower than that in CCM_{HPT}, (~51%), as shown in Fig. 2 (h). This decrease in volume fraction of ε phase in $CCM_{HPTA(1073\ K,0.3\ ks)}$ compared to CCM_{HPT} is attributed to inhomogeneous microstructure caused by HPT processing.

The corresponding IPF maps suggest that the microstruc-

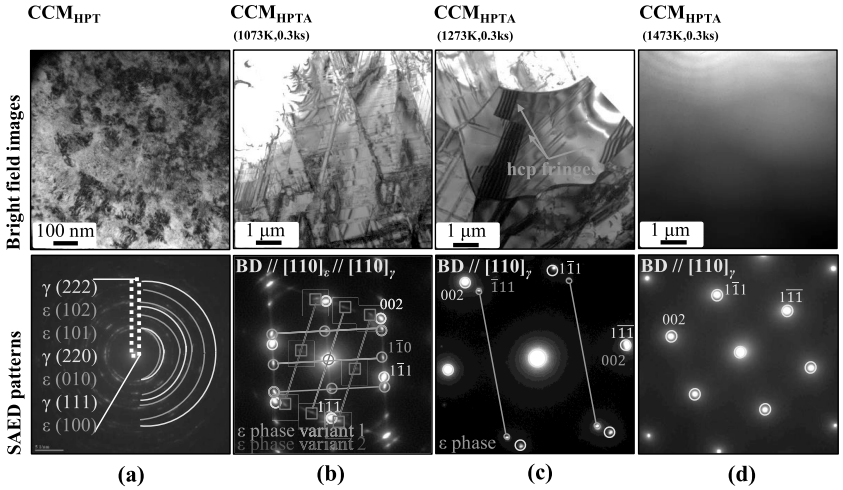

Fig. 3 Transmission electron microscopy (TEM) bright field images and selected area electron diffraction (SAED) patterns of (a) CCM_{HPT}, (b) $CCM_{HPTA(1073\ K,0.3\ ks)}$, (c) $CCM_{HPTA(1273\ K,0.3\ ks)}$ and (d) $CCM_{HPTA(1473\ K,0.3\ ks)}$. γ phase, ε phase variant 1, and ε phase variant 2 are indicated in white, grey (circle) and grey (square), respectively, in the corresponding key diagrams of the SAED patterns. Beam direction is parallel to $[110]_\gamma$ direction.

ture of CCM_{ST} consists of equiaxed grains with an average diameter of ~70 μm, presenting a random orientation distribution. Black areas, which possess a confidence index (CI) smaller than 1, are seen in the IPF map of CCM_{HPT}. It has been reported that these black areas may originate from high strain or nanocrystalline microstructures.[14] Therefore, CCM_{HPT} may show a heterogeneous microstructure consisting of grains in the micrometer and nanometer scale, or grains containing high and low strain. Average grain diameter of γ phase grains in CCM_{HPT} is ~59 μm, while that of ε phase grains is ~65 μm based on EBSD analysis.

These black areas are also observed in the IPF map of CCM_{HPTA} at 1073 K. The average diameter of the visible γ phase grains in $CCM_{HPTA(1073\ K,0.3\ ks)}$ is ~58 μm, while that of the visible ε phase grains is ~62 μm (Fig. 2 (g)). IPF maps of $CCM_{HPTA(1273\ K,0.3\ ks)}$ and $CCM_{HPTA(1473\ K,0.3\ ks)}$ do not show the existence of black areas, but do show recrystallized grains. Average grain diameter in $CCM_{HPTA(1473\ K,0.3\ ks)}$ (~42 μm) is larger than that of $CCM_{HPTA(1273\ K,0.3\ ks)}$ (~6.5 μm), as shown in Fig. 2 (g).

The EBSD KAM maps indicate that the strain of the CCM alloy shows a drastic increase through the HPT processing compared to that of the solution treated (ST) condition. High strain in CCM_{HPT} still exists even though it is subjected to a subsequent short annealing at 1073 K ($CCM_{HPTA(1073\ K,0.3\ ks)}$). Increasing the short annealing temperature causes a decrease in the strain ($CCM_{HPTA(1273\ K,0.3\ ks)}$ and $CCM_{HPTA(1473\ K,0.3\ ks)}$).

Figure 3 shows the TEM bright field images and associated selected area electron diffraction (SAED) patterns including key diagrams of CCM_{HPT}, $CCM_{HPTA(1073\ K,0.3\ ks)}$, $CCM_{HPTA(1273\ K,0.3\ ks)}$, and $CCM_{HPTA(1473\ K,0.3\ ks)}$. Nanocrystalline microstructures at the nanometer scale can be identified in CCM_{HPT}, and their existence is confirmed by the SAED pattern[19,20] in Fig. 3 (a). However, $CCM_{HPTA(1473\ K,0.3\ ks)}$ exhibits a coarse-grained microstructure, and there is no existence of nanometer-scale grains. Two variants of ε plates can be observed in $CCM_{HPTA(1073\ K,0.3\ ks)}$. It is shown that the microstructure of $CCM_{HPTA(1273\ K,0.3\ ks)}$ contains ultrafine grains at the micrometer level and hcp fringes according to Fig. 3 (c).

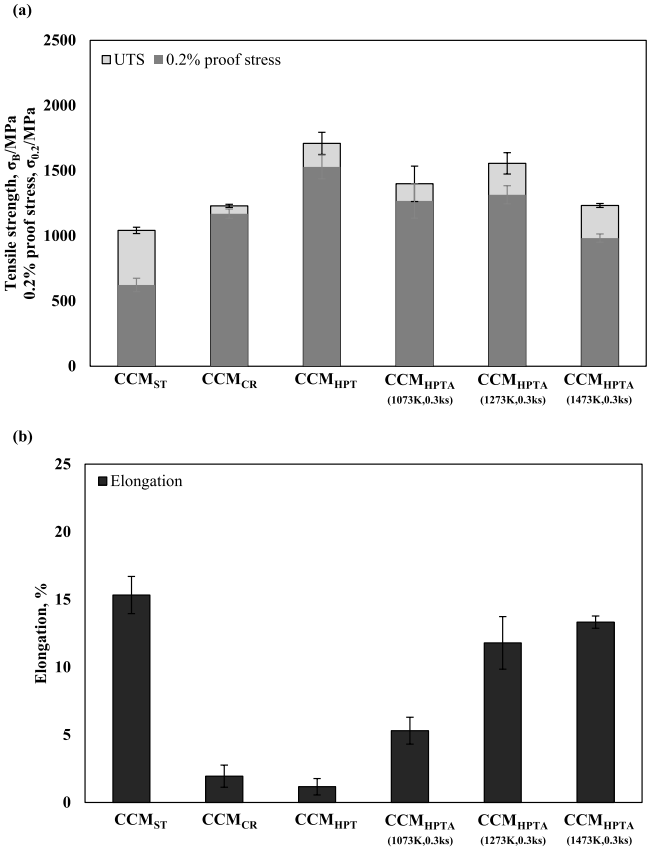

Fig. 4 (a) Tensile strength, 0.2% proof stress and (b) elongation of CCM_{ST}, CCM_{CR}, CCM_{HPT}, $CCM_{HPTA(1073\ K,0.3\ ks)}$, $CCM_{HPTA(1273\ K,0.3\ ks)}$ and $CCM_{HPTA(1473\ K,0.3\ ks)}$.

Tensile properties of CCM_{ST}, CCM_{CR}, CCM_{HPT} and $CCM_{HPTA(1073\ K,0.3\ ks)}$, $CCM_{HPTA(1273\ K,0.3\ ks)}$, and $CCM_{HPTA(1473\ K,0.3\ ks)}$ are shown in Fig 4. The ultimate tensile strength (UTS) and 0.2% proof stress increase through HPT processing at CCM_{HPT} compared to those in the ST condition. However, CCM_{HPT} exhibits poor elongation. Subjecting

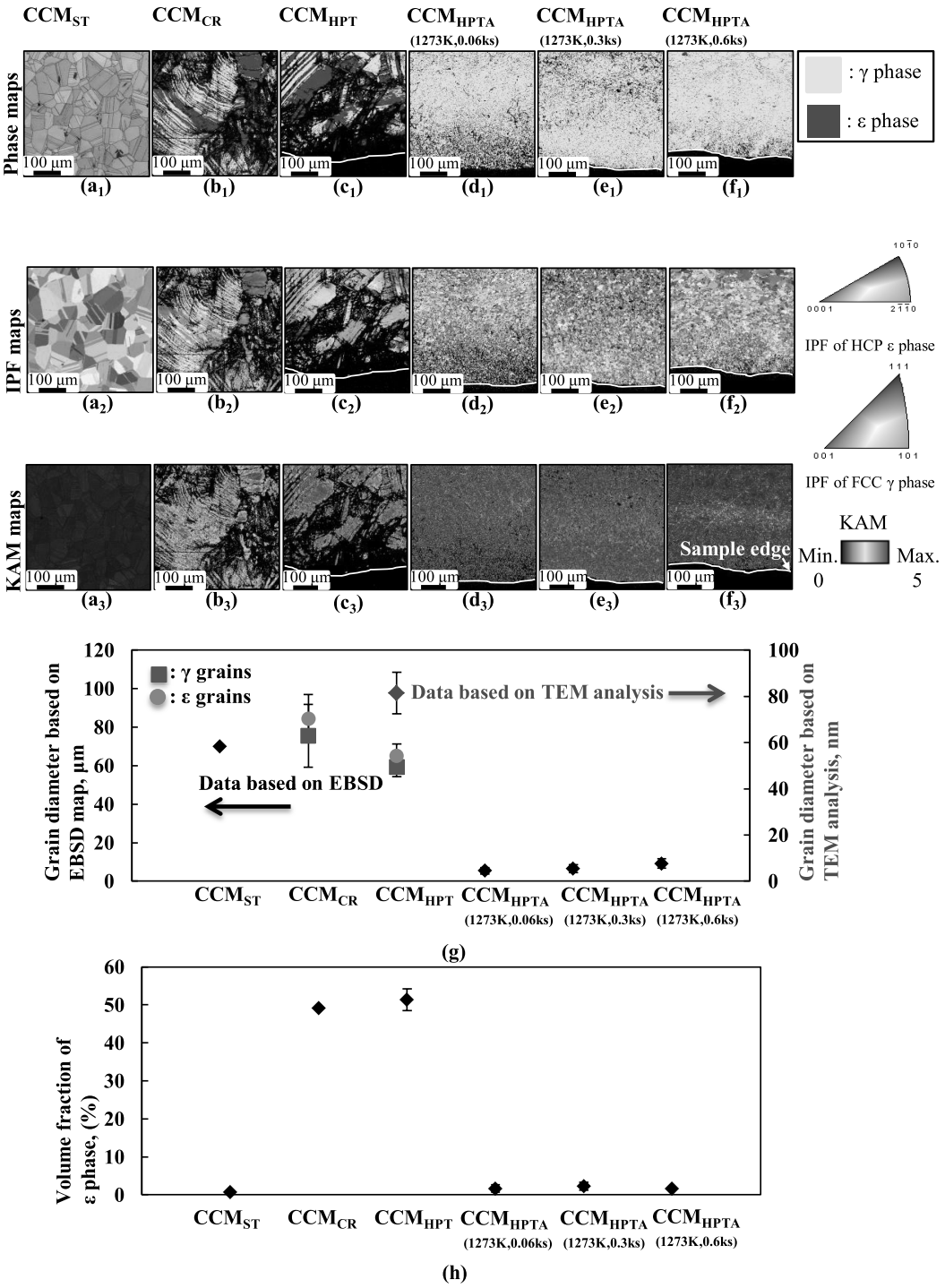

Fig. 5 EBSD ((a$_1$)–(f$_1$)) phase, ((a$_2$)–(f$_2$)) IPF and ((a$_3$)–(f$_3$)) KAM maps and (g) average grain diameter, and (h) volume fraction of ε phases of CCM_{ST}, CCM_{CR}, CCM_{HPT}, and $CCM_{HPTA(1273\ K,0.06\ ks)}$, $CCM_{HPTA(1273\ K,0.3\ ks)}$, and $CCM_{HPTA(1273\ K,0.6\ ks)}$.

CCM_{HPT} to a short annealing causes a decrease in the UTS and 0.2% proof stress. The elongation of CCM_{HPT} is significantly improved with subsequent short annealing of $CCM_{HPTA(1073\ K,0.3\ ks)}$, $CCM_{HPTA(1273\ K,0.3\ ks)}$ and $CCM_{HPTA(1473\ K,0.3\ ks)}$. The UTS and 0.2% proof stress of $CCM_{HPTA(1273\ K,0.3\ ks)}$ are comparable with those of CCM_{HPT}, and higher than those of $CCM_{HPTA(1073\ K,0.3\ ks)}$ and $CCM_{HPTA(1473\ K,0.3\ ks)}$. Therefore, it is realized that the optimum temperature for a short annealing is 1273 K because $CCM_{HPTA(1273\ K,0.3\ ks)}$ exhibits higher tensile strength and larger elongation compared to those of $CCM_{HPTA(1073\ K,0.3\ ks)}$ and $CCM_{HPTA(1473\ K,0.3\ ks)}$.

3.2 Effects of short annealing duration

Figure 5 shows EBSD phase, IPF and KAM maps. Average grain diameter and volume fractions of ε phases of CCM_{ST}, CCM_{CR}, CCM_{HPT}, and $CCM_{HPTA(1273\ K,0.06\ ks)}$, $CCM_{HPTA(1273\ K,0.3\ ks)}$, and $CCM_{HPTA(1273\ K,0.6\ ks)}$. Volume fraction of ε phase is almost constant in CCM_{HPTA} with different annealing duration. Recrystallized grains can be ob-

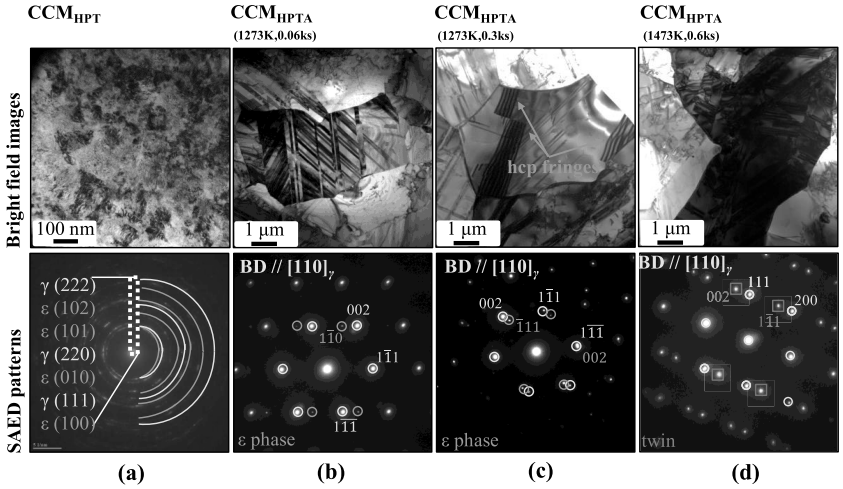

Fig. 6 TEM bright field images and SAED patterns of (a) CCM$_{HPT}$ and (b) CMM$_{HPTA(1273\ K,0.06\ ks)}$, (c) CCM$_{HPTA(1273\ K,0.3\ ks)}$ and (d) CCM$_{HPTA(1273\ K,0.6\ ks)}$. γ phase, γ twin and ε phases are indicated in white, grey (square), and grey (circle), respectively, in the corresponding key diagrams of SAED patterns. Beam direction is parallel to $[110]_\gamma$ direction.

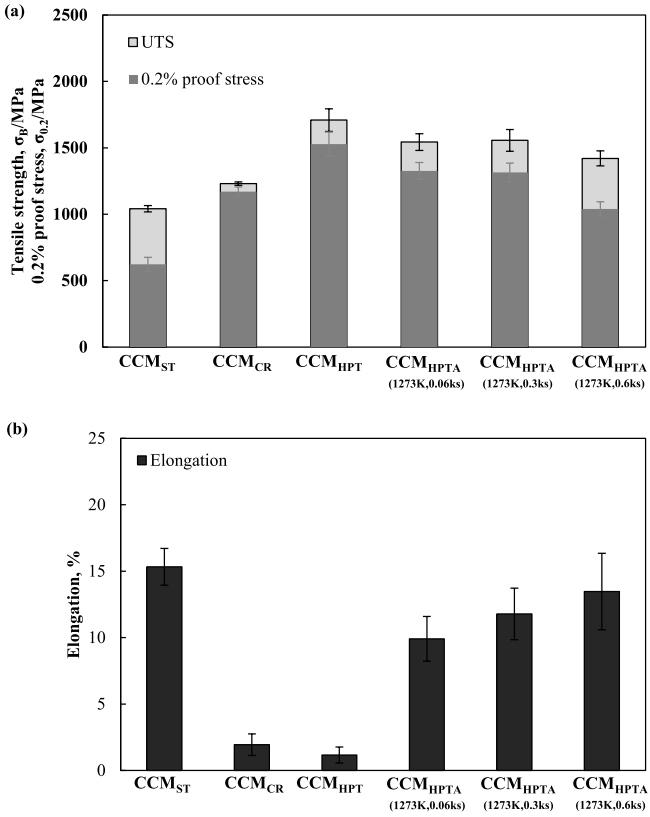

Fig. 7 (a) Tensile strength, 0.2% proof stress and (b) elongation of CCM$_{ST}$, CCM$_{CR}$, CCM$_{HPT}$ and CCM$_{HPTA(1273\ K,0.06\ ks)}$, CCM$_{HPTA(1273\ K,0.3\ ks)}$, and CCM$_{HPTA(1273\ K,0.6\ ks)}$.

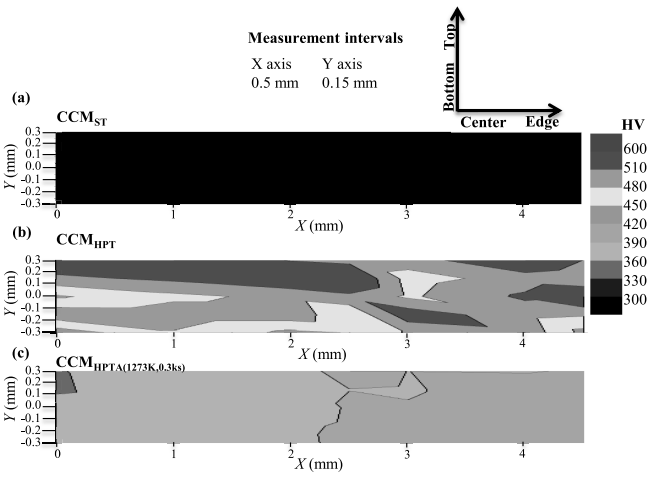

Fig. 8 Hardness distributions in cross sections of (a) CCM$_{ST}$, (b) CCM$_{HPT}$, and (c) CCM$_{HPTA(1273\ K,0.3\ ks)}$.

served in all of the CCM$_{HPTA}$ alloys. Average grain diameter of CCM$_{HPTA}$ increases with increasing short annealing time from 0.06 ks to 0.6 ks. Average grain diameter of CCM$_{HPTA(1273\ K,0.06\ ks)}$, CCM$_{HPTA(1273\ K,0.3\ ks)}$, and CCM$_{HPTA(1273\ K,0.6\ ks)}$ are 5.4 μm, 6.5 μm and 9.2 μm, respectively. Further, the strain in CCM$_{HPTA}$ estimated from KAM value decreases with increasing the short annealing time from 0.3 ks to 0.6 ks based on EBSD KAM maps. Figure 6 shows the TEM bright field images and SAED patterns including key diagrams of CCM$_{HPT}$, CCM$_{HPTA(1273\ K,0.06\ ks)}$, CCM$_{HPTA(1273\ K,0.3\ ks)}$, and CCM$_{HPTA(1273\ K,0.6\ ks)}$. CCM$_{HPT}$ exhibits a nanocrystalline[21] microstructure at the nanometer scale while CCM$_{HPTA}$ exhibits a fine-grained microstructure at the micrometer scale. Two variants of ε plates can be observed in CCM$_{HPT}$, CCM$_{HPTA(1273\ K,0.06\ ks)}$ and CCM$_{HPTA(1273\ K,0.3\ ks)}$. ε martensite plates in CCM$_{HPTA(1273\ K,0.06\ ks)}$ and hcp fringes in CCM$_{HPTA(1273\ K,0.3\ ks)}$ can be observed. CCM$_{HPTA(1273\ K,0.6\ ks)}$ shows a twin microstructure which is confirmed with SAED pattern according to Fig. 6 (d).

Figure 7 shows the tensile properties of CCM$_{ST}$, CCM$_{CR}$, CCM$_{HPT}$, CCM$_{HPTA(1273\ K,0.06\ ks)}$, CCM$_{HPTA(1273\ K,0.3\ ks)}$, and CCM$_{HPTA(1273\ K,0.6\ ks)}$. The UTS and 0.2% proof stress of CCM$_{HPTA}$ do not significantly change with short annealing duration increasing from 0.06 ks to 0.3 ks, and then they show a slight decrease with further increase of time to 0.6 ks. The elongation of CCM$_{HPTA}$ increases gradually with increasing short annealing time. Therefore, it is realized that subject-

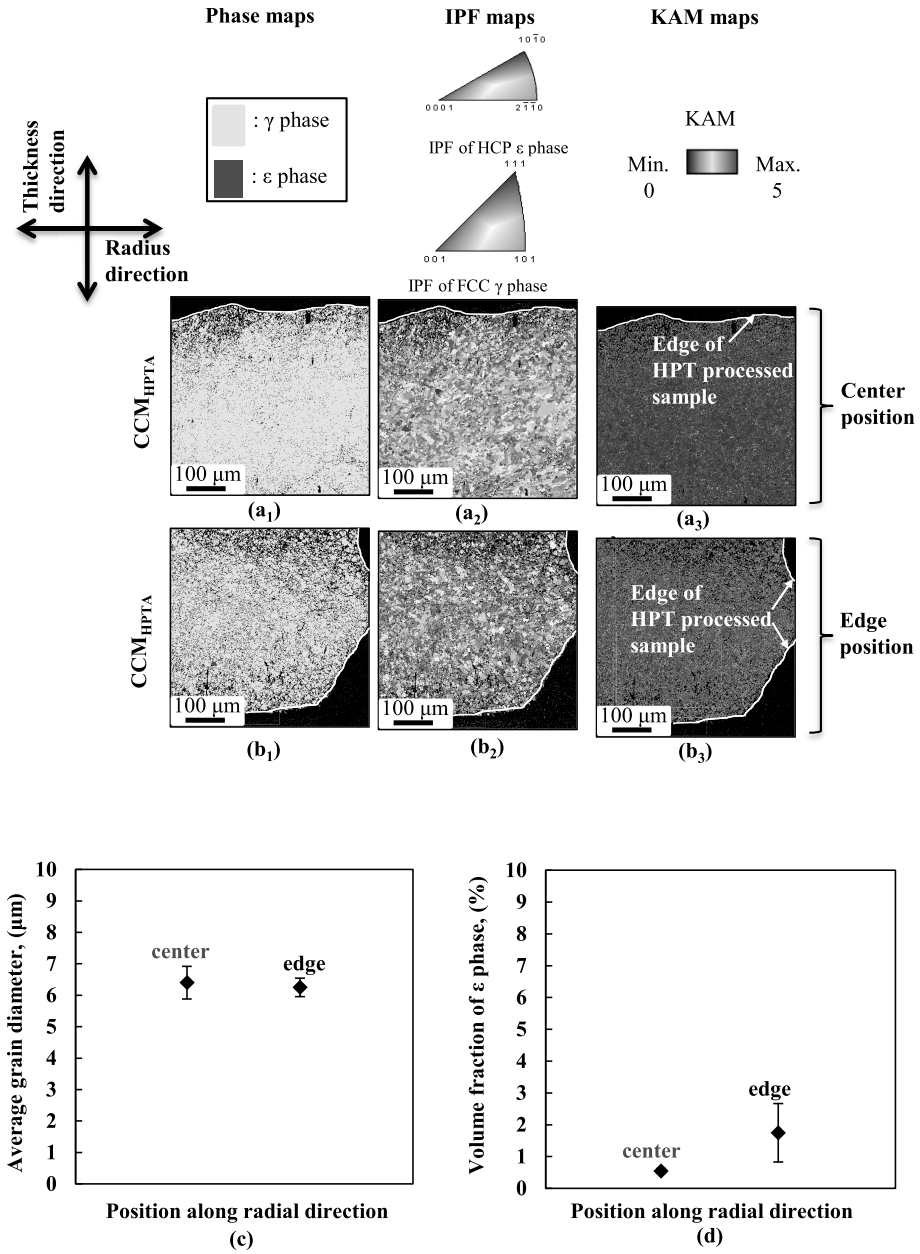

Fig. 9 EBSD ((a_1) and (b_1)) phase, ((a_2) and (b_2)) IPF, and ((a_3) and (b_3)) KAM maps of $CCM_{HPTA(1273\ K,0.3\ ks)}$ at center and edge positions of cross section along radial direction, (c) the evolution of average grain diameter, and (d) volume fraction of ε phase in the cross section as a function of position through radial direction based on EBSD maps in ((a_1) and (b_1)).

ing CCM_{HPT} to a short annealing at 1273 K for 0.3 ks results in high tensile strength and larger elongation compared to those of $CCM_{HPTA(1273\ K,0.06\ ks)}$ and $CCM_{HPTA(1273\ K,0.6\ ks)}$. Optimized properties such as high strength and large elongation are obtained in $CCM_{HPTA(1273\ K,0.3\ ks)}$, which is the best among the short annealing conditions examined. The hardness distribution of $CCM_{HPTA(1273\ K,0.3\ ks)}$ ks is investigated.

3.3 Hardness distribution

Figure 8 shows the hardness distribution for the cross sections of CCM_{ST}, CCM_{HPT}, $CCM_{HPTA(1273\ K,0.3\ ks)}$. Hardness of CCM_{ST} is almost identical and around 300 HV throughout the area of the cross section. Hardness value significantly increases through HPT processing for CCM_{HPT} compared to that of the ST condition. Hardness of CCM_{HPTA} is lower than that of the HPT condition, and it reaches around 360–420 HV. The hardness distribution of CCM_{HPTA} suggests that the hardness is homogenous in the left-half region and right-half regions. In addition, the hardness is slightly higher in the right-half region compared to that of left-half region in CCM_{HPTA}. Therefore, a detailed microstructure analysis was conducted to illuminate the abovementioned phenomenon (EBSD analyses in Fig. 9).

CCM_{HPTA} exhibits a homogeneous hardness distribution on the cross section unlike the CCM_{HPT} as evidenced in EBSD analyses in Fig. 9. The strain and volume fraction of ε phase are slightly larger at the edge of cross section compared to that at the center of cross section of CCM_{HPTA}. Average grain diameters of CCM_{HPTA} at different positions of cross section are almost same.

4. Discussion

4.1 Optimization of short annealing temperature

It is well known that metallic materials are subjected to large strain during HPT processing and this large strain causes the formation of the ε phase in the CCM alloy.[2,13] In γ fcc phase of CCM alloy, with negative stacking fault energy, the glide of Shockley partial dislocations is an elementary deformation step which causes $\varepsilon \rightarrow \gamma$ martensitic transformation. ε-hcp martensitic phase is developed by regular overlapping of the stacking faults on every second $\{1\ 1\ 1\}_\gamma$ plane.[2,13] The volume fraction of the ε phase in the CCM alloy severely increases through HPT processing compared to that of the ST condition (Fig. 2).

Figure 2 shows that the volume fraction of the ε phase in CCM_{HPT} is around 51% according to EBSD analyses. The volume fraction of the ε phase slightly decreases for $CCM_{HPTA(1073\ K,0.3\ ks)}$ compared to that of CCM_{HPT}, and it is around 31% according to Fig. 2. This decrease in volume fraction of ε phase in $CCM_{HPTA(1073\ K,0.3\ ks)}$ compared to CCM_{HPT} is attributed to inhomogeneity of microstructure in specimens caused by HPT processing. Even the microstructure of $CCM_{HPTA(1073\ K,0.3\ ks)}$ is inhomogeneous, excessive amount of ε phase still exists in $CCM_{HPTA(1073\ K,0.3\ ks)}$ and minimization of ε phase could not be achieved in this condition. However, after subjecting CCM_{HPT} to a short annealing at 1273 K and 1473 K, the excessive ε phase can be removed according to Fig. 2.

Figure 2 shows that CCM_{ST} has a coarse-grained microstructure, whereas CCM_{HPT} has visible grains and black areas which may be caused by high strain or grain refinement according to the EBSD maps. A previous study on CCM alloys[14] processed by HPT has reported that grain refinement occurs at CCM alloys processed by HPT to $\varepsilon_{eq} = 4.5$, 9 and 45. Based on the TEM images in Fig. 3 and previous results, it is known that grain refinement also occurred at CCM_{HPT}, which was HPT processed to $\varepsilon_{eq} = 2.25$.

It is shown that $CCM_{HPTA(1073\ K,0.3\ ks)}$ consists of visible grains and black areas similar to those in CCM_{HPT} condition according to Fig. 2. In contrast to the case of CCM_{HPT} (Fig. 3), no ultrafine-grained microstructure was found in TEM images of $CCM_{HPTA(1073\ K,0.3\ ks)}$ although many areas were observed. Therefore, the black areas in the EBSD maps of $CCM_{HPTA(1073\ K,0.3\ ks)}$ are considered to be areas where lattice distortion is too large for EBSD analysis rather than areas where grain size was too small for the EBSD analysis.

In the case of $CCM_{HPTA(1273\ K,0.3\ ks)}$, the occurrence of recrystallization can be identified based on EBSD results in Fig. 2. A new microstructure develops homogeneously throughout the entire specimen. When severely deformed materials with high dislocation density are heated above approximately half of the melting point ($0.5T_m$), recrystallization takes place. Static recovery takes place during the early stage of annealing for the severely deformed materials, which is responsible for the development of recrystallization nuclei as fine dislocation-free crystallites. Grain growth caused by the migration of the boundaries results in consumption of the highly strained microstructure.[22–26] Recrystalization process causes a homogeneous microstructure[27,28] which is consistent with abovementioned corresponding results.

In addition, the refinement of coarse-grains in $CCM_{HPTA(1273\ K,0.3\ ks)}$ is also possible to be occured by short annealing. Previously, it was reported that grain refinement might occur via $\varepsilon \rightarrow \gamma$ reverse transformation via solution treatment. The effect of refinement caused by short annealing exists by some extent[29].

Recrystallization did not occur for $CCM_{HPTA(1073\ K,0.3\ ks)}$. This indicates that the annealing temperature is not enough to achieve recrystallization, even though it was above $0.5T_m$ = ~ 973 K for the CCM alloy. This is because recrystallization is not only determined by the temperature, but also depends on material factors such as the type of lattice, concentration of alloying elements, and size distributions of second phases.[30]

Corresponding results in Fig. 2 also suggest that increasing the temperature for short annealing causes progressive coarsening of the grains for $CCM_{HPTA(1473\ K,0.3\ ks)}$, and the grains become excessively larger compared to those of $CCM_{HPTA(1273\ K,0.3\ ks)}$.

Figure 4 suggests that the UTS and 0.2% proof stress of the CCM alloy increase while the elongation decreases through HPT processing compared to those of CCM_{ST}. Based on previous studies, it can be inferred that HPT processing causes an increase in the tensile strength owing to grain refinement, and an increase in volume fraction of the ε phase and in dislocation density.[14,31–35]

The UTS and 0.2% proof stress of $CCM_{HPTA(1073\ K,0.3\ ks)}$ are lower than to those of the CCM_{HPT}. $CCM_{HPTA(1073\ K,0.3\ ks)}$ exhibits an excessive volume fraction of the ε phase and does not show an ultrafine-grained microstructure, which causes a lower elongation compared to $CCM_{HPTA(1273\ K,0.3\ ks)}$ and $CCM_{HPTA(1473\ K,0.3\ ks)}$.[35,36]

The UTS and 0.2% proof stress of $CCM_{HPTA(1273\ K,0.3\ ks)}$ are higher than those of CCM_{ST}, CCM_{CR}, and $CCM_{HPTA(1473\ K,0.3\ ks)}$, and comparable with those of CCM_{HPT} and $CCM_{HPTA(1073\ K,0.3\ ks)}$. The elongation of $CCM_{HPTA(1273\ K,0.3\ ks)}$ and $CCM_{HPTA(1473\ K,0.3\ ks)}$ is larger than that of other samples except for that of the CCM_{ST}. Therefore, it is concluded that 1273 K is the optimum temperature for a short annealing with the fixed duration of 0.3 ks because of the high strength and large elongation obtained for $CCM_{HPTA(1273\ K,0.3\ ks)}$ compared to those of $CCM_{HPTA(1073\ K,0.3\ ks)}$. In addition, the effect of HPT rotation number ($N = 0.25$, 0.5, 1, 2 and 5) on the mechanical properties of CCM alloy is able to be discussed in this section. It has been reported that tensile strength of CCM_{HPT} almost keeps constant from $N = 0.25$ ($\varepsilon_{eq} = 2.25$) to $N = 1$ ($\varepsilon_{eq} = 9$), then it decreases when N exceeds 1. The elongation of CCM_{HPT} at each rotation number shows a similar value of ~1–2%. Therefore, even though the rotation of 90 degrees ($N = 0.25$) might seem to be rather small, the mechanical properties of CCM_{HPT} at $N = 0.25$ is optimized compared to those of CCM_{HPT} with higher rotation number[14,18]. In this study, the mechanical properties of short annealed CCM_{CR} were not evaluated. The microstructure of short annealed CCM_{CR} was investigated. The average grain diameter was ~41 μm and ε phase with a volume fraction of ~37% could be detected. Therefore, short annealed CCM_{CR} was expected not to exhibit greater mechanical properties due to coarse-grained microstructure and excessive volume fraction of ε phase. Nanocrystalline microstructure cannot be obtained in CCM alloy using cold rolling

process or conventional hot forging[37], while it can be obtained using HPT[14]. Previously, CCM_{HPT} ($N = 0.25$ ($\varepsilon_{eq} = 2.25$)) was compared with hot forged CCM alloy (CCM_{HF}) reported by Yamanaka *et al.*, which has one of the smallest grain diameters among CCM alloys reported in literatures[37]. UTS and 0.2% proof stress of CCM_{HPT} (~1709 MPa and ~1528 MPa) are greater than those of CCM_{HF} (~1450 MPa and ~1330 MPa). In addition, Vickers hardness of CCM_{HPT} at half radius (~503 HV) is greater than that of CCM_{HF} (~428 HV) reported for CCM alloy in practical use[5]. Therefore, it can be concluded that HPT processing helps to achieve greater tensile strength and hardness in CCM alloys than cold rolling and hot forging. The main target of this study was to improve the elongation of CCM_{HPT} and maintain a high strength using a subsequent short annealing, which was used to minimize the ε phase while maintaining nanocrystalline microstructure. Although nanocrystalline microstructure was not able to be maintained with short annealing, the elongation of HPT processed CCM was significantly improved (from (~1% to ~12%) while the UTS (from ~1709 MPa to ~1556 MPa) and 0.2% proof stress (from ~1528 MPa to ~1315 MPa) only relatively slightly decreased.

4.2 Optimization of short annealing duration

The volume fractions of the ε phase are almost 0% in all the CCM_{HPTA} with different annealing times. The average grain diameter of CCM_{HPTA} slightly increases owing to grain growth caused by the migration of the boundaries,[22–26] while strain decreases with increasing short annealing time, which can be identified in Fig. 5.

The UTS and 0.2% proof stress of $CCM_{HPTA(1273\ K,0.06\ ks)}$ and $CCM_{HPTA(1273\ K,0.3\ ks)}$ are almost same according to Fig. 7. This is because the average grain diameter and volume fraction of the ε phase are similar to those of $CCM_{HPTA(1273\ K,0.06\ ks)}$ and $CCM_{HPTA(1273\ K,0.3\ ks)}$. The decrease in UTS and 0.2% proof stress and increase in elongation of $CCM_{HPTA(1273\ K,0.6\ ks)}$ are attributed to an increase in grain size.

4.3 Effect of HPT and subsequent short annealing on hardness distribution

Figure 8 shows that the hardness (HV) of a CCM alloy significantly increases through HPT processing compared to that of CCM_{ST}. This increase in the hardness is attributed to grain refinement, accumulation of dislocations and strain induced martensite.[14,34] CCM_{HPT} exhibits a heterogeneous hardness distribution on the cross section, which is shown in Fig. 8. This heterogeneity in hardness distribution is attributed to the heterogeneous microstructure caused by unusual plastic flow patterns during HPT.[38–40] Hardening occurs at the surface of the HPT processed specimen owing to martensitic transformations, accumulation of dislocation and grain refinement. This hardening may prevent strain from developing deeply below the specimen's surface, causing the heterogeneity in the microstructure.[14]

In the case of CCM_{HPTA}, a homogeneous hardness distribution can be obtained in the left-half region (close to the center) and the right-half region (close to the edge) of the cross section. The hardness of the right-half region is slightly higher than that of the left-half region. The increase in the strain and the volume fraction of the ε phase at the edge of the specimen compared to that in the center of the specimen can be identified in Fig. 9. This result can explain the increase in hardness at the edge of the CCM_{HPTA} specimen.

5. Conclusions

In this study, a CCM alloy was subjected to HPT processing and a subsequent short annealing under various conditions in order to optimize its mechanical properties. The microstructure and mechanical properties were investigated. The obtained results are as follows:

(1) $\gamma \rightarrow \varepsilon$ martensitic transformation and grain refinement induced by HPT processing increase the tensile strength of the CCM alloy. However, HPT processing decreases the elongation.

(2) An optimized mechanical property, which is a combination of high strength and large elongation, is achieved for $CCM_{HPTA(1273\ K,0.3\ ks)}$. This is attributed to the minimization of the volume fraction of the ε phase and maintaining the fine-grained microstructure in $CCM_{HPTA(1273\ K,0.3\ ks)}$.

(3) Subjecting CCM_{HPT} to a short annealing at 1273 K for 0.3 ks causes a decrease in hardness (HV) but a more homogeneous hardness distribution compared to those of CCM_{HPT}.

Acknowledgements

This study was supported in part by a Grant-in-Aid for Scientific Research (A) No. 24246111 from the Japan Society for the Promotion of Science (JSPS) and the Inter-University Cooperative Research Program "Innovation Research for Biosis-Abiosis Intelligent Interface" from the Ministry of Education, Culture, Sports, Science and Technology (MEXT), Japan. The HPT process was carried out in the International Research Center on Giant Straining for Advanced Materials (IRC-GSAM) at Kyushu University.

REFERENCES

1) S.H. Sun, Y. Koizumi, S. Kurosu, Y.P. Li, H. Matsumoto and A. Chiba: Acta Mater. **64** (2014) 154–68.
2) K. Yamanaka, M. Mori and A. Chiba: Acta Biomater. **9** (2013) 6259–67.
3) A. Chiba, K. Kumagai, N. Nomura and S. Miyakawa: Acta Mater. **55** (2007) 1309–18.
4) Y. Koizumi, S. Suzuki, K. Yamanaka, B.S. Lee, K. Sato, Y. Li, S. Kurosu, H. Matsumoto and A. Chiba: Acta Mater. **61** (2013) 1648–61.
5) Y. Koizumi, Y. Chen, Y. Li, K. Yamanaka, A. Chiba, S.I. Tanaka and Y. Hagiwara: Mater. Sci. Eng. C **62** (2016) 532–543.
6) K. Yamanaka, M. Mori, S. Kurosu, H. Matsumoto and A. Chiba: Metall. Mater. Trans., A **40** (2009) 1980–1994.
7) P.W. Bridgman: Phys. Rev. **48** (1935) 825–847.
8) P.H.R. Pereira, R.B. Figueiredo, P.R. Cetlin and T.G. Langdon: Mater. Sci. Eng. A **631** (2015) 201–8.
9) R.Z. Valiev and T.G. Langdon: Prog. Mater. Sci. **51** (2006) 881–981.
10) A.P. Zhilyaev and T.G. Langdon: Prog. Mater. Sci. **53** (2008) 893–979.
11) H. Yilmazer, M. Niinomi, K. Cho, M. Nakai, J. Hieda, S. Sato and Y. Todaka: Acta Mater. **80** (2014) 172–82.
12) R.B. Figueiredo and T.G. Langdon: Mater. Sci. Eng. A **528** (2011) 4500–4506.
13) K.Yamanaka, M. Mori, Y. Koizumi, and A. Chiba: J. Mech. Behav. Biomed. Mater., 2014, vol. **32**, pp. 52–61.
14) M. Isik, M. Niinomi, K. Cho, H. Liu, M. Nakai, H. Yilmazer, Z. Horita and T. Narushima: J. Mech. Behav. Biomed. Mater. **59** (2016) 226–35.
15) H. Matsumoto, S. Kurosu, B.S. Lee, Y. Li and A. Chiba: Scr. Mater. **63**

(2010) 1092–1095.
16) H. Matsumoto, Y. Koizumi, T. Ohashi, B.S. Lee, Y. Li and A. Chiba: Acta Mater. **64** (2014) 1–11.
17) R. Ueji, N. Tsuji, T. Ohashi, Y. Minamino and Y. Koizumi: Sci. Technol. Adv. Mater. **5** (2004) 153–162.
18) M. Isik, M. Niinomi, H. Liu, K. Cho, M. Nakai, Z. Horita, T. Narushima, H. Yilmazer and M. Nagasako: Mater. Trans. **57** (2016) 1109–1118.
19) D.K. Yang, P. Cizek, P.D. Hodgson and C.E. Wen: Acta Mater. **58** (2010) 4536–48.
20) N. Hansen: Scr. Mater. **51** (2004) 751–53.
21) Q. Wei, S. Cheng, K.T. Ramesh and E. Ma: Mater. Sci. Eng. A **381** (2004) 71–79.
22) F. J. Humphreys and M. Hatherly: *Recrystallization and related phenomena*, Australia, 2004.
23) R. D. Doherty, D. A. Hughes, F. J. Humphreys, J. J. Jonas, D. J. Jensen, M. E. Kassner, W. E. King, T. R. McNelley, H. J. McQueen, and A.D. Rollett: Mater. Today, 1998.
24) J.E. Burke and D. Turnbull: Prog. Met. Phys. **3** (1952) 220–92.
25) J.E. Bailey: Proc. Roy. Soc. (London), Ser. A **267** (1962) 11–30.
26) T. Sakai, A. Belyakov, R. Kaibyshev, H. Miura and J.J. Jonas: Prog. Mater. Sci. **60** (2014) 130–207.
27) E. Hornbogen and U. Koster: *Dr. Riederer-Verlag, Gmbh (Stuttgart)*, 1978, pp. 159–94.
28) H. Ahlborn, E. Hornbogen and U. Köster: J. Mater. Sci. **4** (1969) 944–50.
29) S. Kurosu, H. Matsumoto and A. Chiba: Mater. Lett. **64** (2010) 49–52.
30) J. R. Davis and A.S.M.I.H. Committee: *Nickel, Cobalt, and Their Alloys*, ASM International, 2000.
31) P.H.R. Pereira, R.B. Figueiredo, P.R. Cetlin and T.G. Langdon: Mater. Sci. Eng. A **631** (2015) 201–8.
32) S. Gourdet and F. Montheillet: Acta Mater. **51** (2003) 2685–99.
33) Y. Mine, S. Matsumoto and Z. Horita: Corros. Sci. **53** (2011) 2969–77.
34) R.Z. Valiev, E.V. Kozlov, Y.F. Ivanov, J. Lian, A.A. Nazarov and B. Baudelet: Acta Metall. Mater. **42** (1994) 2467–75.
35) T. Mitsunobu, Y. Koizumi, B.S. Lee, K. Yamanaka, H. Matsumoto, Y. Li and A. Chiba: Acta Mater. **81** (2014) 377–85.
36) K. Edalati, S. Toh, M. Arita, M. Watanabe and Z. Horita: Appl. Phys. Lett. **102** (2013) 181902–181906.
37) K. Yamanaka, M. Mori and A. Chiba: Mater. Sci. Eng. A **528** (2011) 5961–5966.
38) Y. Cao, Y.B. Wang, S.N. Alhajeri, X.Z. Liao, W.L. Zheng, S.P. Ringer, T.G. Langdon and Y.T. Zhu: J. Mater. Sci. **45** (2010) 765–70.
39) R.B. Figueiredo and T.G. Langdon: Mater. Sci. Eng. A **528** (2011) 4500–4506.
40) M. Kawasaki, R.B. Figueiredo and T.G. Langdon: Acta Mater. **59** (2011) 308–16.